Structural, magnetic, and Mössbauer spectral study of the icosahedral quasicrystal $Zn_{77}Fe_7Sc_{16}$

K. Al-Qadi,[1] P. Wang,[1] Z. M. Stadnik,[1,*] and J. Przewoźnik[2]
[1]*Department of Physics, University of Ottawa, Ottawa, Ontario, Canada K1N 6N5*
[2]*Department of Solid State Physics, Faculty of Physics and Applied Computer Science, AGH University of Science and Technology, 30-059 Kraków, Poland*

(Received 3 February 2009; revised manuscript received 14 May 2009; published 8 June 2009)

The structural, magnetic, and Mössbauer spectral properties of the icosahedral quasicrystal $Zn_{77}Fe_7Sc_{16}$ are reported. The thermodynamically stable quasicrystal $Zn_{77}Fe_7Sc_{16}$ has a primitive six-dimensional Bravais lattice at room temperature with a six-dimensional hypercubic lattice constant of 7.087(1) Å. Based on dc magnetization measurements, no evidence is found for a transition to a ground state with long-range magnetic order in the temperature range between 2 and 300 K. The dc zero-field-cooled and field-cooled susceptibility data indicate that the studied quasicrystal is a spin glass with freezing temperature T_f=7.75(2) K. This is further confirmed by observing aging effects through the dc zero-field-cooled magnetization and the thermoremanent magnetization time decays and by the analysis of the frequency dependence of T_f using the Vogel-Fulcher law and the dynamic scaling behavior near T_f. However, the observed increase in the thermoremanent magnetization with the magnetic field in the low-field regime is incompatible with the ultrametrically organized phase space of a canonical spin glass. The nature of the spin-glass state of the icosahedral quasicrystal $Zn_{77}Fe_7Sc_{16}$ is therefore fundamentally different from that of a canonical spin glass. The bimodal distribution of the electric quadrupole splitting and of the hyperfine magnetic field derived from Mössbauer spectra indicates the existence of two classes of Fe sites.

DOI: 10.1103/PhysRevB.79.224202 PACS number(s): 61.44.Br, 75.50.Kj, 75.50.Lk, 76.80.+y

I. INTRODUCTION

Solids are traditionally divided into two groups: crystalline and amorphous. The dramatic discovery of an icosahedral Al-Mn alloy in 1984 by Shechtman *et al.*[1] extended this dichotomous division by introducing the notion of quasicrystals (QCs). These are compounds that possess a new type of long-range translational order, quasiperiodicity, and noncrystallographic orientational order associated with the classically forbidden fivefold, eightfold, tenfold, and twelvefold symmetry axes.[2] A central problem in condensed-matter physics is determining whether quasiperiodicity leads to physical properties which are significantly different from those of crystalline and amorphous materials of the same/similar compositions.

One of the main questions in the physics of QCs is that of the possibility of the existence of long-range magnetic order in these alloys. The initial intuition suggests that quasiperiodicity necessarily leads to geometrical frustration and is therefore incompatible with long-range magnetic order. However, the symmetry-based arguments clearly show[3] that quasiperiodicity does not disallow long-range magnetic order in QCs. In addition, theoretical considerations based on the Ising model,[4] the *XY* model,[5] the Heisenberg model,[6] and the Hubbard model[7] lead to the possibility of the existence of long-range magnetic order in these alloys.

On the experimental side, all known QCs are either diamagnets, paramagnets, or spin glasses.[8] The recent claim[9] of the existence of long-range magnetic order in icosahedral (*i*)*R*-Mg-Zn (*R*=rare earth) QCs was shown[10] to result from the presence of magnetic impurities in the studied samples. Recent extensive neutron-diffraction studies[11] of *i*-*R*-Mg-Zn and *i*-*R*-Mg-Cd QCs, which are of very high structural quality and which can be produced in single-grain form, revealed the presence of short-range spin correlations at low temperatures and the absence of long-range magnetic order; these QCs are spin glasses.

Recently, new thermodynamically stable *i* QCs were discovered in the Zn-TM-Sc (TM=transition-metal) system.[12] These QC's are formed by replacing some of the Zn in the binary 1/1 approximant Zn_6Sc (Ref. 13) with the TM. As the 1/1 approximant Cd_6Yb to the thermodynamically stable binary *i*-$YbCd_{5.7}$ QC is isostructural with Zn_6Sc, it is expected that the structure of the *i*-Zn-TM-Sc QCs must be similar to that of the *i*-$YbCd_{5.7}$ QC. The crystal structure of the *i*-$YbCd_{5.7}$ QC has been solved very recently.[14] It is based on three building units (rhombic triacontahedra linked with acute and obtuse rhombohedra) arranged quasiperiodically with unique atomic decorations. One would expect that Sc and TM atoms are distributed among the Yb sites (on the vertices of the icosahedron and inside the acute rhombohedron) and the Zn atoms are located at the Cd sites.

The new *i*-Zn-TM-Sc QCs could possibly possess sizeable 3*d* magnetic moments on the TM atoms[15] and perhaps exhibit long-range magnetic order. It is therefore of interest to determine the magnetic properties of these new QC's. We report in this paper on structural, magnetic, and ^{57}Fe Mössbauer spectroscopy (MS) studies of the *i* alloy $Zn_{77}Fe_7Sc_{16}$.

II. EXPERIMENTAL METHODS

As starting elements, Zn shots (purity 99.999%), Fe foil (purity 99.99%), and Sc chunks (purity 99.9%) were used as received; Fe element was enriched to 95.4% in the ^{57}Fe isotope. Appropriate amounts of these elements corresponding to the composition $Zn_{77}Fe_7Sc_{16}$ were weighed (±0.1 mg) and weld sealed under an argon atmosphere into a tantalum container. The container was in turn held within an evacuated

SiO_2 jacket to avoid its air oxidation. The mixture was melted at 1000 °C for 2 h, followed by annealing at 700 °C for 120 h.

X-ray diffraction (XRD) measurements were performed at 298 K in Bragg-Brentano geometry on the PANanalytical X'Pert scanning diffractometer using Cu $K\alpha$ radiation. The $K\beta$ line was eliminated by using a Kevex PSi2 Peltier-cooled solid-state Si detector. In order to avoid deviation from intensity linearity of the solid-state Si detector, its parameters and the parameters of the diffractometer were chosen in such a way as to limit the count rate from the most intense Bragg peaks to less than 9000 counts/s.[16] To allow for possible instrumental aberration and specimen displacement, corrections were made to the 2θ angles using a fourth-order polynomial calibration curve[17] obtained from a scan of the specimen mixed with 10 wt % of a Si standard.[18]

The dc magnetic susceptibility was measured with a Quantum Design superconducting quantum interference device (SQUID) magnetometer at various magnetic fields in the temperature range of 2.0–300 K. The sample in chunk form (the linear size of the chunks was about 0.5 mm) was placed in a low-background fused silica sample holder of geometry similar to that described by Lewis and Bussmann.[19] Our sample holder consisted of an unsealed fused silica tube at the center of which a fused silica cylindrical container (a cup with a lid) was sandwiched between two smaller fused silica tubes. The bottom of the outer tube was narrowed to hold the inner structure in place. The gap between the cup and the lid was smaller than the size of the sample chunks inside the cup; this ensured that the sample could not accidentally leave the cup and that it was in direct thermal contact with a He gas flowing inside the silica tubes. The ac magnetic susceptibility data were collected in a Quantum Design physical property measurement system between 2.0 and 30 K in a 1 Oe ac magnetic field and zero external dc magnetic field for frequencies varying from 20 Hz to 10 kHz. The sample in a disk form was securely anchored to a low-background sample holder.

The ^{57}Fe MS measurements in the temperature range of 1.9–289.4 K were conducted using a standard Mössbauer spectrometer operating in sine mode and a ^{57}Co(Rh) source at room temperature. The spectrometer was calibrated with a 6.35-μm-thick α-Fe foil,[20] and the spectra were folded. The full linewidth at half maximum of the inner pair of the α-Fe Zeeman pattern was 0.210(2) mm/s, and this value can be regarded as the resolution of the Mössbauer spectrometer. The Mössbauer absorber consisted of a mixture of pulverized material and boron nitride, which were pressed into a pellet that was put into an Al disk container of thickness 0.008 mm to ensure a uniform temperature over the whole absorber. The surface densities of the Mössbauer absorbers of the i-$Zn_{77}Fe_7Sc_{16}$ QC were 1.10 and 1.21 mg ^{57}Fe/cm^2 for measurements below and above 4.2 K, respectively.

III. RESULTS AND DISCUSSION

A. Structural characterization

The XRD pattern of the sample measured in the 2θ range of 5–90° (Fig. 1) shows the presence of 39 i Bragg peaks.

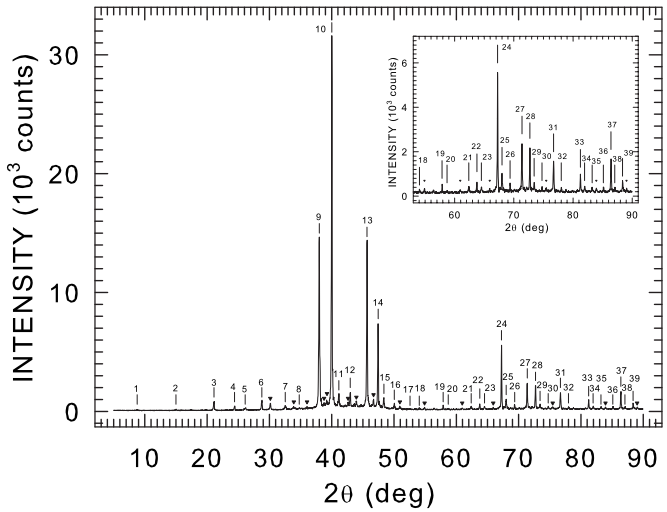

FIG. 1. The XRD pattern of the i-$Zn_{77}Fe_7Sc_{16}$ quasicrystal at 298 K corrected for the Cu $K\alpha_2$ lines. The vertical lines labeled with integers above all detected i Bragg peaks correspond to the positions calculated for the Cu $K\alpha_1$ radiation, as explained in the text. The inset shows a magnification of the low-intensity region. The position, full width at half maximum, and relative area of each detected i peak are given in Table I together with the corresponding index. The symbol ▼ indicates the peak positions corresponding to an unidentified second phase.

Bragg peaks of very small intensity due to an unidentified second phase are also observed (Fig. 1). The positions of all the detected i Bragg peaks corresponding to $K\alpha_1$ radiation [the value of its wavelength λ is 1.540 598 1 Å (Ref. 21)] in terms of the angle $2\theta_1$ and the corresponding wave number $Q_{exp}=4\pi \sin \theta_1/\lambda$, as well as their relative intensities and full widths at half maximum Γ_Q, were determined from the profile fitting using the procedure described by Schreiner and Jenkins.[22] These parameters, corresponding to 39 detected i peaks, whose positions are indicated by vertical lines in Fig. 1, are presented in Table I. This table also contains the theoretical positions Q_{cal} which were calculated by taking the position of the second most intense i peak as the reference. Since there are several schemes employed to index the i peaks, we present in Table I the indices that correspond to the most frequently used schemes.[23–25]

The form of indices of the observed i Bragg peaks (Table I) shows that the i-$Zn_{77}Fe_7Sc_{16}$ QC has a primitive six-dimensional Bravais lattice. There is good agreement between the observed Q_{exp} and theoretical Q_{cal} positions of the i Bragg peaks (Fig. 1 and Table I). The value of the six-dimensional hypercubic lattice constant calculated from the value Q_{exp} that corresponds to the (18,29) i peak is 7.087(1) Å. The width Γ_Q of most of the i peaks is very narrow: for example, Γ_Q=0.009 Å^{-1} corresponding to the (52/84) i Bragg peak (Table I) is nearly equal to that of the (400) Bragg peak of the Si standard (0.008 Å^{-1}) measured with the same x-ray diffractometer. This is indicative of a high degree of structural order of the studied QC.

TABLE I. Positions in terms of $2\theta_1$(in degrees) corresponding to Cu $K\alpha_1$ radiation and Q_{exp} (in $\mathrm{Å}^{-1}$), full width at half maximum Γ_Q (in $\mathrm{Å}^{-1}$), and relative area A normalized to 100.0 of all detected icosahedral Bragg peaks. Q_{exp} (in $\mathrm{Å}^{-1}$) is the calculated Q value by taking the position of the ninth line with the $I1$ index 18/29 as the reference line. $I1$ and $I2$ are the indices (N/M) and $(h/h',k/k',l/l')$ based on the indexing scheme of Cahn *et al.* (Ref. 23), whereas $I3$ and $I4$ are the indices corresponding, respectively, to the indexing schemes of Elser (Ref. 24) and Bancel *et al.* (Ref. 25).

Label	$2\theta_1$	Q_{exp}	Q_{cal}	Γ_Q	A	$I1$	$I2$	$I3$	$I4$
1	8.791	0.625	0.627	0.016	0.1	2/1	011000	100000	$21\bar{1}\bar{1}\bar{1}1$
2	15.002	1.065	1.067	0.011	0.3	4/4	000200	110000	$2200\bar{1}1$
3	21.098	1.493	1.495	0.014	3.0	6/9	011200	111000	110001
4	24.401	1.724	1.726	0.011	1.2	8/12	002200	111100	$1100\bar{1}0$
5	26.108	1.842	1.836	0.017	0.9	10/13	122100	111110	$2210\bar{2}0$
6	28.791	2.028	2.029	0.008	1.9	12/16	022200	211000	$31\bar{1}\bar{1}\bar{1}1$
7	32.547	2.286	2.283	0.015	1.5	14/21	102300	211100	$2100\bar{1}1$
8	34.792	2.439	2.441	0.007	0.2	16/24	222200	211110	$210\bar{1}\bar{1}1$
9	38.002	2.656	2.656	0.014	51.5	18/29	122300	211111	100000
10	40.017	2.791	2.792	0.012	100.0	20/32	002400	221001	110000
11	41.145	2.866	2.862	0.015	5.0	22/33	012410	221101	$2210\bar{1}1$
12	42.970	2.988	2.989	0.010	3.7	24/36	022400	222000	$2211\bar{1}1$
13	45.677	3.166	3.167	0.011	43.6	26/41	013400	222100	111101
14	47.473	3.283	3.283	0.008	5.7	28/44	222400	311111	210001
15	48.368	3.342	3.342	0.009	2.6	30/45	102500	321001	$3200\bar{1}1$
16	50.041	3.450	3.452	0.010	1.3	32/48	004400	321101	$320\bar{1}\bar{1}1$
17	52.564	3.612	3.607	0.015	0.3	34/53	122500	321111	220001
18	54.057	3.707	3.709	0.008	0.3	36/56	013510	322100	$2210\bar{1}0$
19	57.878	3.947	3.949	0.009	0.8	40/64	242400	322111	111100
20	58.713	3.999	3.999	0.014	0.3	42/65	104500	322200	$310\bar{1}\bar{1}1$
21	62.383	4.224	4.222	0.010	1.0	46/73	013600	332001	$2110\bar{1}0$
22	63.765	4.308	4.310	0.009	1.3	48/76	233510	332101	$2110\bar{1}1$
23	64.520	4.354	4.355	0.010	0.7	50/77	213600	332111	320002
24	67.248	4.517	4.518	0.009	12.0	52/84	004600	332002	101000
25	67.994	4.561	4.562	0.011	2.4	54/85	253400	422111	221101
26	69.361	4.641	4.642	0.007	0.6	56/88	024600	333100	$3100\bar{1}1$
27	71.375	4.758	4.759	0.010	7.5	58/93	233600	333101	210000
28	72.718	4.836	4.837	0.008	5.4	60/96	224600	422211	$210\bar{1}00$
29	73.430	4.876	4.877	0.009	0.9	62/97	015600	432101	$320\bar{1}\bar{1}0$
30	74.755	4.952	4.953	0.006	0.2	64/100	253510	432111	$3210\bar{1}1$
31	76.706	5.061	5.062	0.009	4.0	66/105	104700	432002	$2111\bar{1}1$
32	78.010	5.134	5.135	0.005	0.2	68/108	114710	432102	221001
33	81.243	5.311	5.312	0.008	1.7	72/116	244600	433101	200000
34	81.953	5.349	5.348	0.009	0.6	74/117	235600	433111	$2220\bar{1}0$
35	83.229	5.417	5.418	0.007	0.4	76/120	015710	433200	320001
36	85.128	5.517	5.518	0.010	0.5	78/125	344601	433201	211001
37	86.399	5.584	5.585	0.007	3.2	80/128	004800	442002	220000
38	87.055	5.618	5.620	0.007	0.2	82/129	144700	442102	$3211\bar{1}1$
39	88.367	5.685	5.686	0.008	1.3	84/132	024800	522221	$320\bar{1}02$

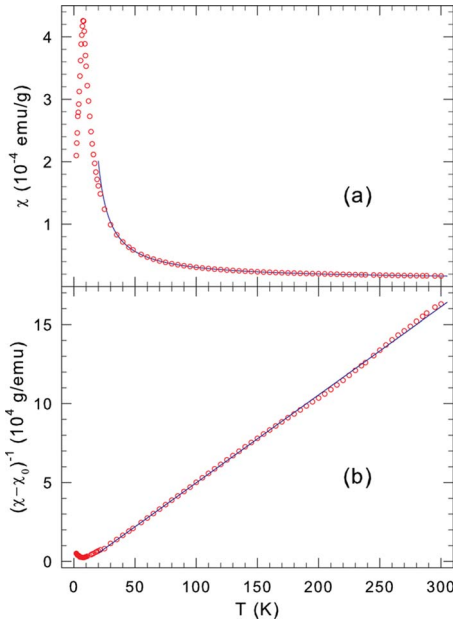

FIG. 2. (Color online) (a) The temperature dependence of the magnetic susceptibility of the i-$Zn_{77}Fe_7Sc_{16}$ quasicrystal, measured in an external magnetic field of 50 Oe. The solid line is the fit to Eq. (1) in the temperature range of 40–300 K, as explained in the text. (b) The inverse magnetic susceptibility corrected for the contribution χ_0 $(\chi-\chi_0)^{-1}$ versus temperature T of the i-$Zn_{77}Fe_7Sc_{16}$ quasicrystal. The solid line is the fit to Eq. (1).

B. Magnetic measurements

1. dc magnetic susceptibility

The magnetic susceptibility χ of the i-$Zn_{77}Fe_7Sc_{16}$ QC measured in an applied magnetic field of 50 Oe between 2.0 and 300 K is shown in Fig. 2(a). The sample was zero-field cooled (ZFC) to 2.0 K, and the measurement was performed while warming the sample up to 300 K. The $\chi(T)$ curve exhibits a definite peak at 7.74(4) K indicating magnetic ordering. The $\chi(T)$ data above 40 K could be fitted to a modified Curie-Weiss law,

$$\chi = \chi_0 + \frac{C}{T-\Theta_p}, \tag{1}$$

where χ_0 is the temperature-independent magnetic susceptibility, C is the Curie constant, and Θ_p is the paramagnetic Curie temperature. The Curie constant can be expressed as $C=\frac{N\mu_{\rm eff}^2}{3k_B}$, where N is the concentration of magnetic atoms per unit mass, $\mu_{\rm eff}$ is the effective magnetic moment, and k_B is the Boltzmann constant. Figure 2(b) shows the inverse magnetic susceptibility corrected for the contribution χ_0 $(\chi-\chi_0)^{-1}$ versus temperature. The values of χ_0, C, and Θ_p obtained from the fit are, respectively, $1.07(1)\times10^{-5}$ emu/g $[9.40(9)\times10^{-3}$ emu/(mol Fe)], $1.80(1)\times10^{-3}$ emu K/g $[1.58(1)$ emu K/(mol Fe)], and 10.6(2) K. This value of C corresponds to $\mu_{\rm eff}$ of 3.55(1) μ_B per Fe atom.

For a metallic compound, the temperature-independent magnetic susceptibility χ_0 is expected to consist of two contributions: the diamagnetic susceptibility of core electrons and the Pauli susceptibility of conduction electrons, $\chi_0=\chi_d+\chi_P$. The diamagnetic contribution χ_d in an alloy is usually estimated as a weighted average of the susceptibilities of the constituents of the alloy. Using the diamagnetic susceptibilities for metallic Zn, Fe, and Sc,[26] one finds that $\chi_d=-0.31\times10^{-3}$ emu/(mol Fe). This gives the Pauli susceptibility of $9.71(9)\times10^{-3}$ emu/(mol Fe). The derived value of χ_P is significantly larger than the largest values [on the order of 1×10^{-3} emu/(mol Fe)] for Fe-containing compounds[27,28] and is comparable to the χ_P values for heavy-fermion systems.[29] The most probable reason for the large value of χ_P found here is the contribution to χ_0 of unidentified impurity/impurities present in our sample.

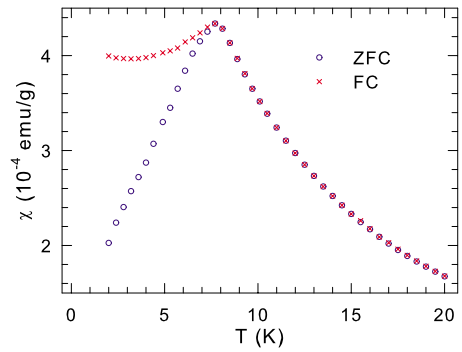

FIG. 3. (Color online) The temperature dependence of the ZFC and FC magnetic susceptibility of the i-$Zn_{77}Fe_7Sc_{16}$ quasicrystal, measured in an external magnetic field of 50 Oe.

The positive value of Θ_p indicates the predominantly ferromagnetic interaction between the Fe atoms. The magnetic moment of 3.55 μ_B per Fe atom is the highest ever reported for a stable QC containing a TM element.[8,15] Recent electronic structure calculations[30] for a cubic approximant to the i-$Zn_{77}Fe_7Sc_{16}$ QC predict the magnetic moment per Fe atom in the range of 1.2–2.4 μ_B.

To determine the nature of the magnetic transition at 7.74 K, we measured the temperature dependence of the ZFC and field-cooled (FC) magnetic susceptibility around 8.0 K in an applied magnetic field of 50 Oe (Fig. 3). The occurrence of a bifurcation between the ZFC and FC data at the freezing temperature T_f=7.75(2) K is evident. Above T_f both ZFC and FC data are identical. Such a behavior of the ZFC and FC susceptibility data is characteristic of a spin glass.[31] The i-$Zn_{77}Fe_7Sc_{16}$ QC is thus a spin glass with a freezing temperature T_f=7.75(2) K.

2. Relaxation effects in the dc magnetization

An aging phenomenon, which was discovered by Lundgren *et al.*,[32] is an inherent characteristic of a spin-glass system. The measurement of aging effects in spin glasses is carried out either via the ZFC magnetization decay measurement or the complementary thermoremanent magnetization (TRM) decay measurement.[31] The first involves cooling the sample in zero magnetic field from above T_f to the measuring temperature T_m below T_f, allowing the sample to stay at T_m for a certain waiting time t_w, and then applying a small magnetic field and recording the change in magnetization with time. The second utilizes cooling the sample in a small

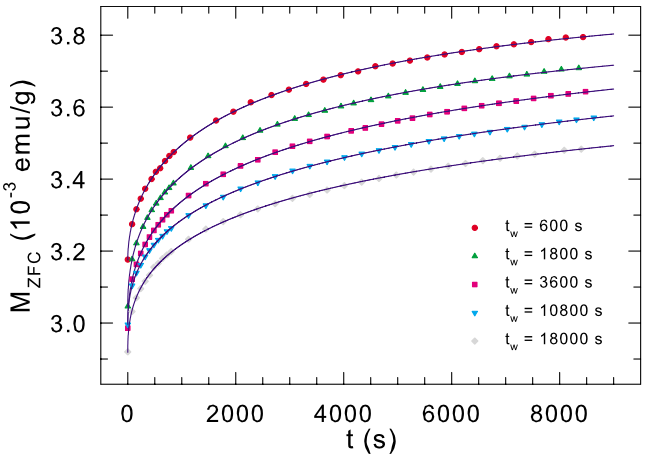

FIG. 4. (Color online) The time dependence of the ZFC magnetization for an applied magnetic field of 20 Oe at 4.8 K for different waiting times t_w of the i-$Zn_{77}Fe_7Sc_{16}$ quasicrystal. The solid lines are the fits to Eq. (2).

magnetic field from above T_f to T_m below T_f, keeping the sample at T_m for a time t_w, and then rapidly removing the magnetic field and recording the change in magnetization with time. The dependence of the magnetization decays on t_w is called aging.

Figure 4 shows the ZFC magnetization decays at $T_m = 4.8$ K$=0.62T_f$ and in 20 Oe for different waiting times. It is clear from the figure that the measured ZFC magnetization strongly depends on t_w: the longer the t_w, the slower the decay of the ZFC magnetization. The system becomes "stiffer" for larger waiting times. This confirms the existence of aging processes in the i-$Zn_{77}Fe_7Sc_{16}$ QC. The observed dependence of the ZFC magnetization on t_w is the same as that observed for canonical spin glasses.[31]

Among the various functional forms that have been proposed to describe the magnetization decay, one of the most successful in describing the data is a stretched exponential of the form

$$M(t) = M_0 - M_r \exp\left[-\left(\frac{t}{\tau_r}\right)^{1-n}\right], \qquad (2)$$

where M_0 relates to an intrinsic ferromagnetic component, M_r is a glassy component, τ_r is the characteristic time constant, and n is the stretched exponential exponent.[33] The time constant τ_r and the exponent n are related to the relaxation rate of the spin glass. The data could be well fitted to Eq. (2) as evidenced by the solid lines in Fig. 4. The values of the fitted parameters are listed in Table II. Within experimental error, n and M_r are independent of t_w, whereas τ_r increases with t_w. The independence of n and M_r of t_w was observed for canonical spin glasses.[33,34]

The aging phenomenon in the i-$Zn_{77}Fe_7Sc_{16}$ QC was also studied by the TRM decay measurements. Figure 5 shows the TRM decays for different waiting times at a cooling field of 50 Oe and at $T_m=4.8$ K$=0.62T_f$ and $T_m=6.0$ K$=0.77T_f$. The following observations follow from the data (Fig. 5): (1) the TRM decreases substantially as T_f is approached; (2) the larger the t_w, the larger the TRM; (3) and the time decay of the TRM slows down as t_w increases. These three dependencies are precisely the same as those observed for canonical spin glasses[33–36] and can be explained within the context of an ultrametric organization of the metastable states in a spin glass.[35,36]

TABLE II. Results of a fit to Eq. (2) of ZFC magnetization decays at $T=4.8$ K and $H=20$ Oe for different waiting times t_w.

t_w (s)	M_0 (10^{-3} emu/g)	M_r (10^{-3} emu/g)	τ_r (10^3 s)	n
600	3.93(3)	0.77(8)	3.08(2)	0.467(95)
1800	3.87(3)	0.83(5)	3.14(2)	0.519(43)
3600	3.90(3))	0.92(4)	5.08(8)	0.555(23)
10800	3.87(4)	0.88(4)	7.53(11)	0.550(23)
18000	3.80(5)	0.88(4)	7.84(12)	0.576(27)

The ultrametric topology of the metastable states was predicted by Parisi[37] and co-workers[38] via replica-symmetry solution of the Sherrington-Kirkpatrick infinite-range spin-glass model.[39] A pure state α of a spin glass is characterized by the thermal average magnetization at a site i, m_i^α. An overlap function between two states α and β is $q^{\alpha\beta} = N^{-1}\Sigma_{i=1}^N m_i^\alpha m_i^\beta$, where N is the total number of spins, which are assumed here to be of Ising type. The self-overlap $q^{\alpha\alpha}$ is the Edwards-Anderson (EA) order parameter,[40] and it fulfills

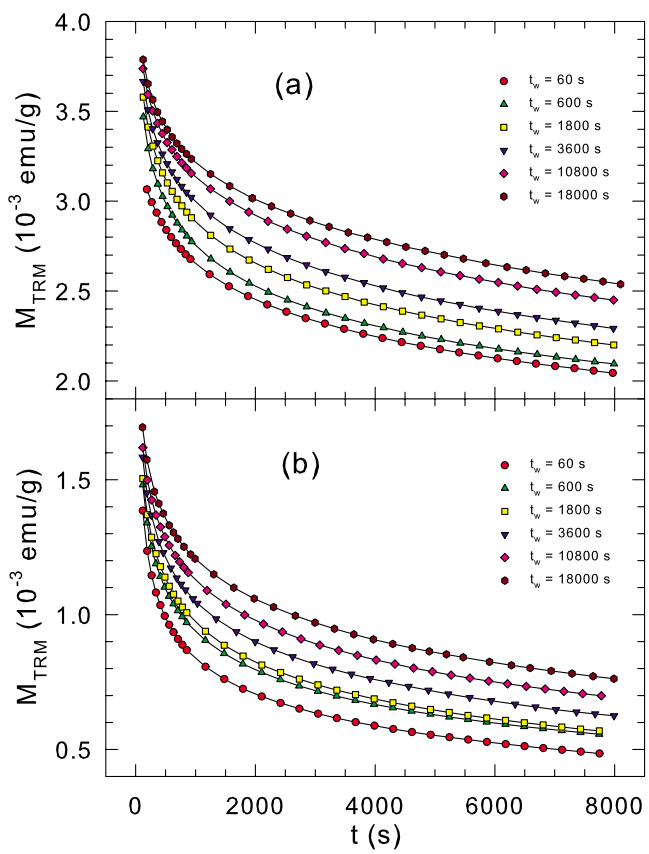

FIG. 5. (Color online) The TRM time decays at $H=50$ Oe for the different waiting times t_w at (a) 4.8 and (b) 6.0 K of the i-$Zn_{77}Fe_7Sc_{16}$ quasicrystal. The solid lines are guides for the eyes.

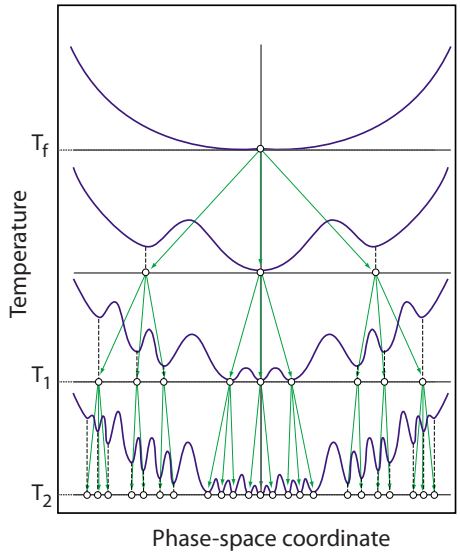

FIG. 6. (Color online) The hierarchical organization of the metastable states in a spin glass. The coarse-grained free-energy surface is represented at each level corresponding to a given temperature. When the temperature is decreased ($T_2 < T_1 < T_f$), each valley subdivides into others. Aging refers to jumping of the system over ever increasing energy barriers during the waiting time t_w.

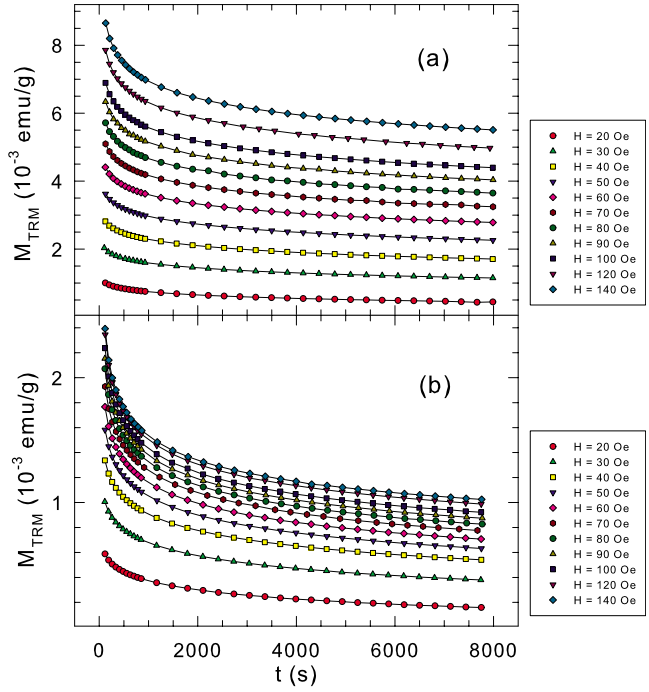

FIG. 7. (Color online) The TRM time decays for t_w=3600 s at (a) 4.8 and (b) 6.0 K for different cooling fields H of the i-$Zn_{77}Fe_7Sc_{16}$ quasicrystal. The solid lines are guides for the eyes.

the relation $-q_{EA}(T) \leq q^{\alpha\beta} \leq q_{EA}(T)$. The number N_S of metastable states, or equivalently the number of relative minima of the free energy, is equal to the number of solutions to the Thouless-Anderson-Palmer equations.[41] Close to T_f, N_S increases exponentially with T as[42] $N_S = \exp[(8/81)N \times (1-T/T_f)^6]$. As a result, the complexity of the free-energy landscape in configuration space increases dramatically with decreasing T. It was shown[38,43] that the structure of the organization of the metastable states obeys a property called ultrametricity: for any three states α, β, and γ, having mutual overlaps $q^{\alpha\beta}$, $q^{\alpha\gamma}$, and $q^{\beta\gamma}$, at least two of the overlaps are equal and the third is larger than or equal to the other two. This property can be represented as a hierarchical treelike organization of the states[44] (Fig. 6). As the temperature is lowered from, say, T_1 to T_2 ($T_2 < T_1 < T_f$), a given metastable state α at T_1 gives "birth" to N_α new states at T_2.

The three dependencies of the TRM observed here for the studied i-$Zn_{77}Fe_7Sc_{16}$ QC and for canonical spin glasses can be explained[35,36] within the framework of the ultrametric organization of the metastable states (Fig. 6). When the spin system is cooled to T_m in the magnetic field H, it explores during the waiting time t_w different metastable states in the phase space by jumping over the energy barriers. Assuming that the jumps occur via a thermally activated process, the part of the phase space explored is characterized by the highest surmounted energy barrier Δ_{max} that depends on T_m and t_w and is given by $\Delta_{max}(T_m, t_w) = T_m \ln(\frac{t_w}{\tau})$, where τ is a macroscopic attempt time. At the end of the waiting time t_w, the magnetic field is reduced from H to zero, and the TRM decay is measured. Here, two closely related processes take place. First, a new set of metastable states with zero magnetization replaces the set of the metastable states with magnetization M_{FC} as the ground state. Second, this results in a "tilt" in the free-energy surface which rapidly empties those occupied states with M_{FC} with energy barriers less than or equal to the change in Zeeman energy, HM_{FC}. This accounts for the rapid change in the magnetization (so-called reversible part) upon cutting the magnetic field H to zero. For longer times, the diffusion process from occupied states with M_{FC} with energy barriers larger than HM_{FC} to the states with zero magnetization occurs. This leads to the slow decay of the so-called irreversible part of the magnetization (TRM). For longer waiting times, the weight of the populated FC phase space bounded by energy barriers larger than the change in Zeeman energy increases, and consequently, the magnitude of the TRM should increase. Moreover, because of a larger fraction of states surrounded by higher energy barriers for longer waiting time, it takes a longer time for the system to leave these states and decay toward the "sink" among low-barrier heights which have been overcome by HM_{FC}. This explains why the decay of the TRM is slower for longer waiting times.

The existence of the ultrametrically organized phase space in a spin glass can also be evidenced by studying the TRM decay as a function of the cooling field H, which should be in the low-field region where the ZFC and FC magnetizations differ substantially.[36] The decay of the TRM for t_w=3600 s at T_m=4.8 K=0.62T_f and T_m=6.0 K=0.77T_f as a function of the cooling field H is shown in Fig. 7. It is clear from Fig. 7 that the magnitude of the TRM increases with the cooling field. The TRM dependence on H observed here is exactly *opposite* to that observed for a canonical spin glass where the TRM decreases with H. The decrease in the TRM with H is expected for the ultrametrically organized phase space in a spin glass:[36] the larger the cooling field H, the smaller the region of populated states bounded by barriers of height

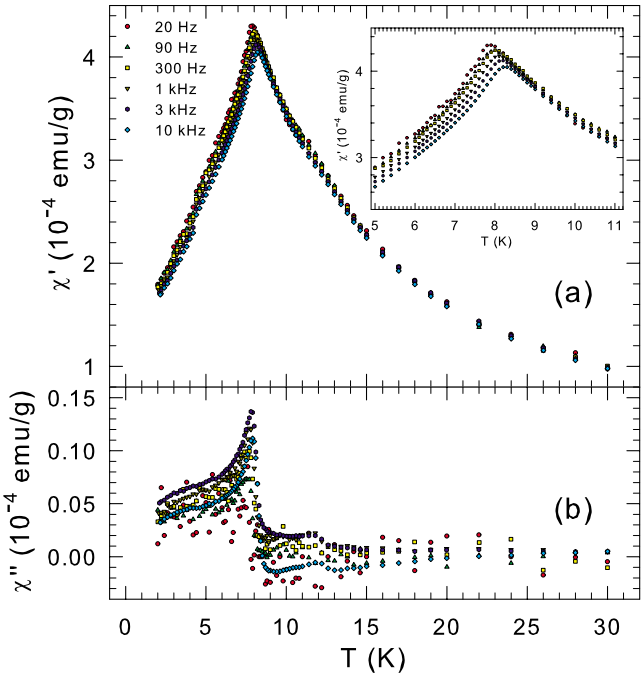

FIG. 8. (Color online) The temperature dependence of the (a) in-phase magnetic susceptibility χ' and (b) out-of-phase magnetic susceptibility χ'' measured for different applied frequencies from 20 Hz to 10 kHz for the i-$Zn_{77}Fe_7Sc_{16}$ quasicrystal. The inset in (a) is a magnification around the maximum in χ'

$\Delta(t_w) > HM_{FC}$ so that a smaller TRM remains after $H \to 0$. We thus have to conclude that the observed increase in the TRM with H in the i-$Zn_{77}Fe_7Sc_{16}$ QC is inconsistent with the ultrametrically organized phase space. This result contradicts the spin-glass nature of the ground state in the i-$Zn_{77}Fe_7Sc_{16}$ QC in the sense of a canonical spin glass.

3. ac magnetic susceptibility

The in-phase component χ' and the out-of-phase component χ'' of the ac magnetic susceptibility for i-$Zn_{77}Fe_7Sc_{16}$ QC, measured in the temperature range from 2 to 30 K and for selected frequencies between 20 Hz and 10 kHz, are shown in Figs. 8(a) and 8(b), respectively. Both $\chi'(T)$ and $\chi''(T)$ curves show maxima whose amplitudes and positions depend on the frequency f of the applied ac magnetic field.

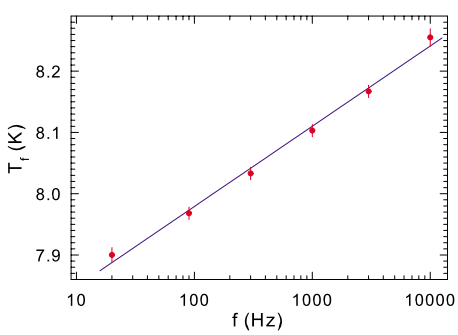

FIG. 9. (Color online) The frequency dependence of the freezing temperature T_f for the i-$Zn_{77}Fe_7Sc_{16}$ quasicrystal. The solid line is the best linear fit to the T_f data.

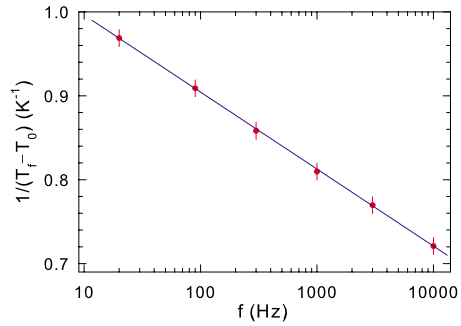

FIG. 10. (Color online) The frequency dependence of the freezing temperature T_f for the i-$Zn_{77}Fe_7Sc_{16}$ quasicrystal. The solid line is the best fit to Eq. (4).

There is a sharp peak in $\chi'(T)$ which can be used to define T_f. $\chi'(T)$ attains a maximum at T_f that shifts toward higher temperatures with higher frequencies, which is typical for conventional spin glasses.[31] Below the maximum, the magnitude of χ' is frequency dependent, but it becomes independent of frequency at temperatures just above T_f. This behavior is qualitatively similar to that of conventional spin glasses.[31] The out-of-phase component χ'' is vanishing above T_f but is nonzero for temperatures just below T_f, which implies dissipation not only at the freezing transition but also for temperatures below it, a common feature of spin glasses.[31]

The frequency dependence of T_f, which was determined from the maximum of the data in Fig. 8(a), obtained by curve fitting, is shown in Fig. 9. A quantitative measure of the change in the freezing temperature with frequency in spin glasses is represented by the relative change in T_f per decade change in f defined as[31]

$$K = \frac{\Delta T_f}{T_f \Delta \log f}. \tag{3}$$

From a linear fit of the data in Fig. 9, and using the average value of T_f=8.08 K for the range of frequencies used, we find that K=0.016(1). This value is a factor of 3 greater than that observed for the canonical $Cu_{1-x}Mn_x$ spin glass but comparable to that of several other canonical spin glasses.[31] We note that the value of K reported for another i-$Tb_9Mg_{34}Zn_{57}$ QC is 0.049.[45]

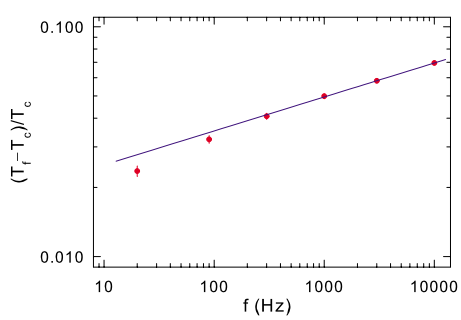

FIG. 11. (Color online) The frequency dependence of the freezing temperature T_f for the i-$Zn_{77}Fe_7Sc_{16}$ quasicrystal. The solid line is the best fit to Eq. (5).

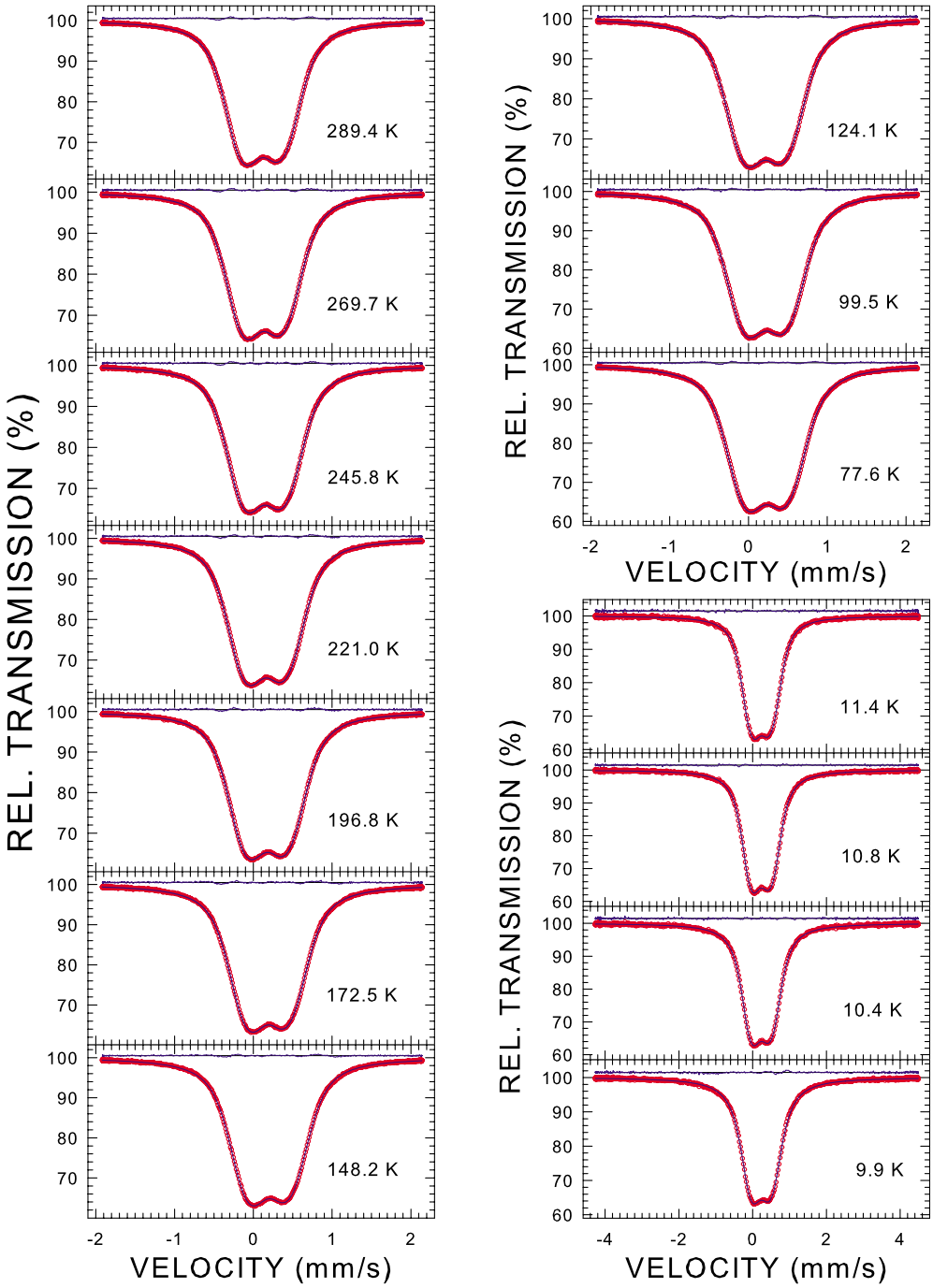

FIG. 12. (Color online) The ^{57}Fe Mössbauer spectra of the i-$Zn_{77}Fe_7Sc_{16}$ quasicrystal obtained at the indicated temperatures fitted (solid lines) with the quadrupole splitting distributions $P(\Delta)$ shown in Fig. 13. The residuals are shown above each spectrum. The zero-velocity origin is relative to α-Fe at room temperature.

There are basically two different interpretations of the spin freezing phenomenon in spin glasses:[31] one is a cluster model in which the system is considered as a set of interacting superparamagnetic clusters and the other is a model which assumes the occurrence of a true phase transition. The frequency dependence of T_f in spin glasses is described within the cluster model by the phenomenological Vogel-Fulcher law,[31,46]

$$f = f_0 \exp[-E_a/k_B(T_f - T_0)], \tag{4}$$

where f_0 is a characteristic frequency, E_a is the activation energy, and T_0 is the Vogel-Fulcher temperature which is a measure of the interaction strengths between clusters in the spin glass.[47] Equation (4) implies a linear dependence of $1/(T_f - T_0)$ on $\log(f)$. The best fit of the $T_f(f)$ data to Eq. (4) (Fig. 10) yields $f_0 = 7.20(22) \times 10^{11}$ Hz, E_a/k_B

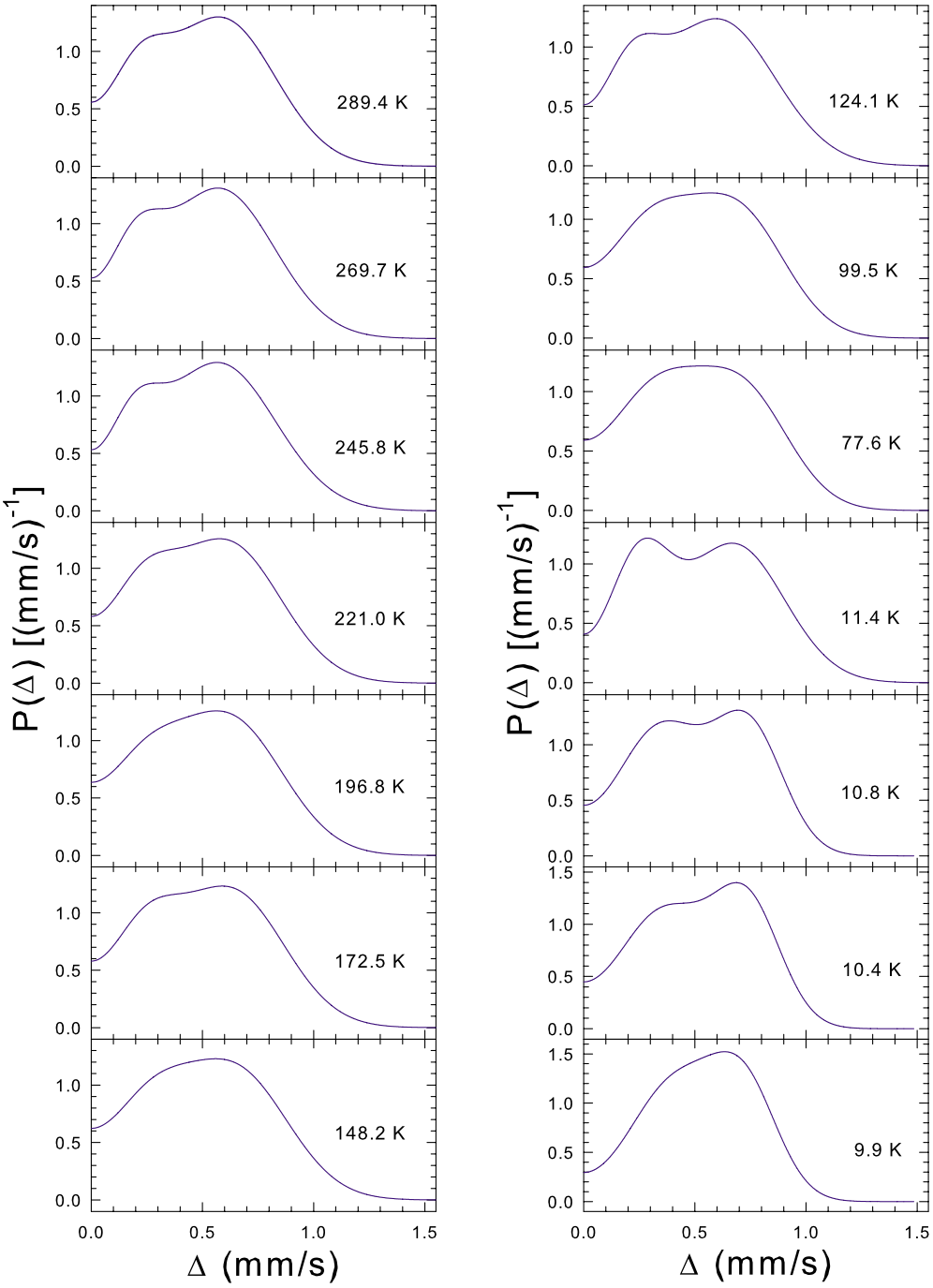

FIG. 13. (Color online) The quadrupole splitting distributions $P(\Delta)$ which fit best the ^{57}Fe Mössbauer spectra in Fig. 12.

=25.1(2.6) K, and T_0=6.87(47) K. Similar to what was observed for other spin glasses,[46] $T_0 < E_a/k_B$. The values of f_0, E_a/k_B, and T_0 obtained for the i-$Zn_{77}Fe_7Sc_{16}$ QC are in general agreement with similar parameters reported for other spin-glass systems.[31,45,46]

The frequency-dependent maximum of $\chi'(T)$ indicates the freezing temperature T_f where the maximum relaxation time, τ, of the system is equal to the characteristic time $1/f$ set by the frequency of the ac-susceptibility measurement. The scaling theory near a phase transition at T_c predicts that the temperature dependence of τ obeys the power-law divergence,[31,48]

$$\tau = \tau_0 \left(\frac{T_f - T_c}{T_c} \right)^{-z\nu}, \quad T_f > T_c, \tag{5}$$

where τ_0 is the microscopic relaxation time, z is the dynamic exponent relating the correlation length ξ and τ as $\tau \propto \xi^z$, and ν is the critical exponent for the correlation length $\xi \propto (\frac{T_f}{T_c} - 1)^{-\nu}$. The best fit of the $T_f(f)$ data to Eq. (5) (Fig. 11) gives $\tau_0 = 1.47(32) \times 10^{-12}$ s, T_c=7.72(8) K, and $z\nu$=6.77(1.14). The derived values of τ_0 and $z\nu$ are similar to those for the canonical $Cu_{1-x}Mn_x$ spin glass.[31,49]

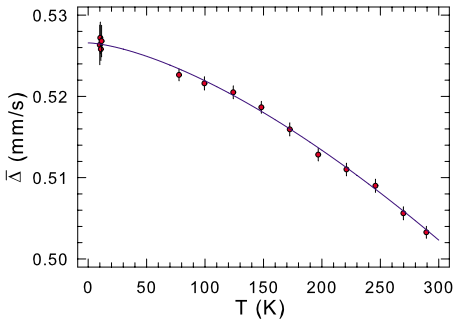

FIG. 14. (Color online) The temperature dependence of the average quadrupole splitting of the i-$Zn_{77}Fe_7Sc_{16}$ quasicrystal. The solid line is the fit to Eq. (7).

C. Mössbauer spectroscopy

The Mössbauer spectra of the i-$Zn_{77}Fe_7Sc_{16}$ QC recorded at temperatures at which no magnetic dipole hyperfine interaction[50] is present are shown in Fig. 12. All the spectra consist of a broadened doublet which results from the distribution of the quadrupole splitting, $P(\Delta)$,[51] a quadrupole splitting that is given by

$$\Delta = \frac{1}{2} eQ|V_{zz}|\sqrt{1+\eta^2/3}, \tag{6}$$

where e is the proton charge and Q is the electric quadrupole moment of the ^{57}Fe nucleus. The asymmetry parameter $\eta = |(V_{xx}-V_{yy})/V_{zz}|$, $(0 \leq \eta \leq 1)$, where V_{xx}, V_{yy}, and V_{zz} are the eigenvalues of the electric field gradient (EFG) tensor in order of increasing magnitude.[50] The distribution $P(\Delta)$ is the consequence of the distributions of the EFG and of the asymmetry parameter. The Mössbauer spectra in Fig. 12 were fitted with the Voigt-based quadrupole distribution method of Rancourt and Ping.[52] To account for a small asymmetry of the spectra, a linear coupling between the center shift, δ, and

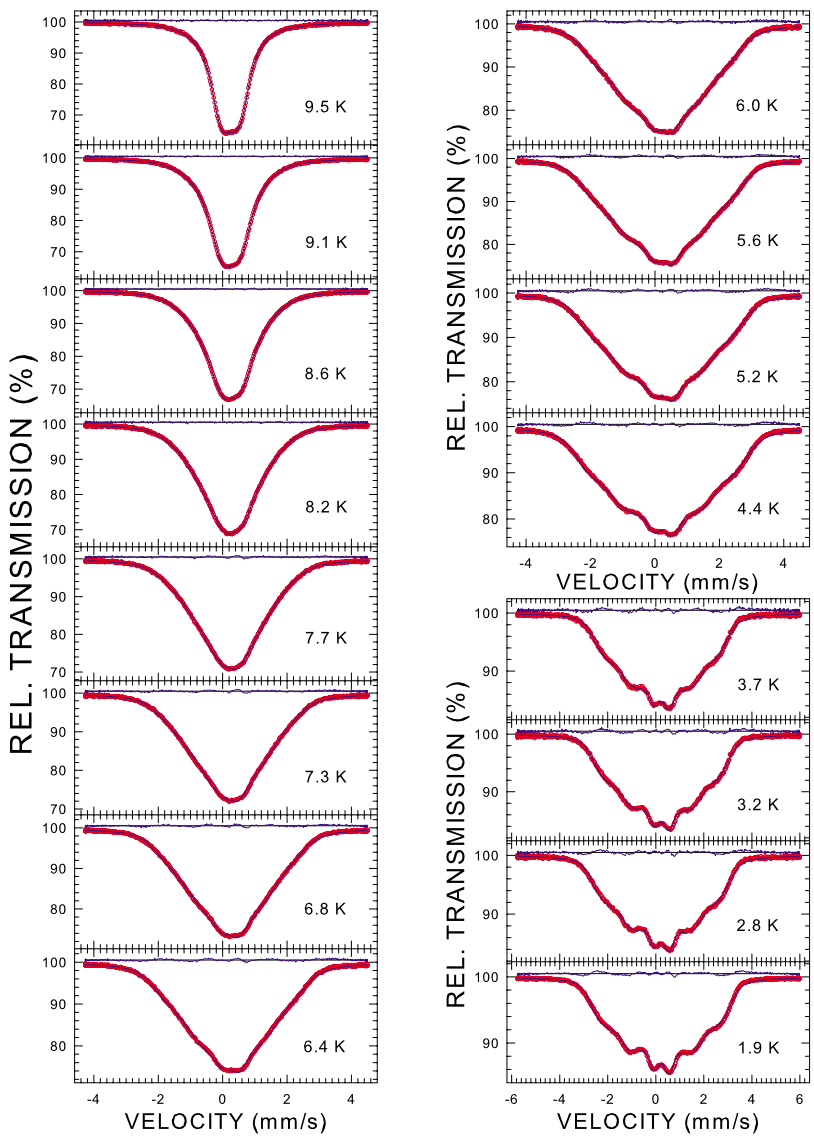

FIG. 15. (Color online) The ^{57}Fe Mössbauer spectra of the i-$Zn_{77}Fe_7Sc_{16}$ quasicrystal obtained at the indicated temperatures fitted (solid lines) with the hyperfine magnetic field distributions $P(H_{hf})$ shown in Fig. 16. The residuals are shown above each spectrum. The zero-velocity origin is relative to α-Fe at room temperature.

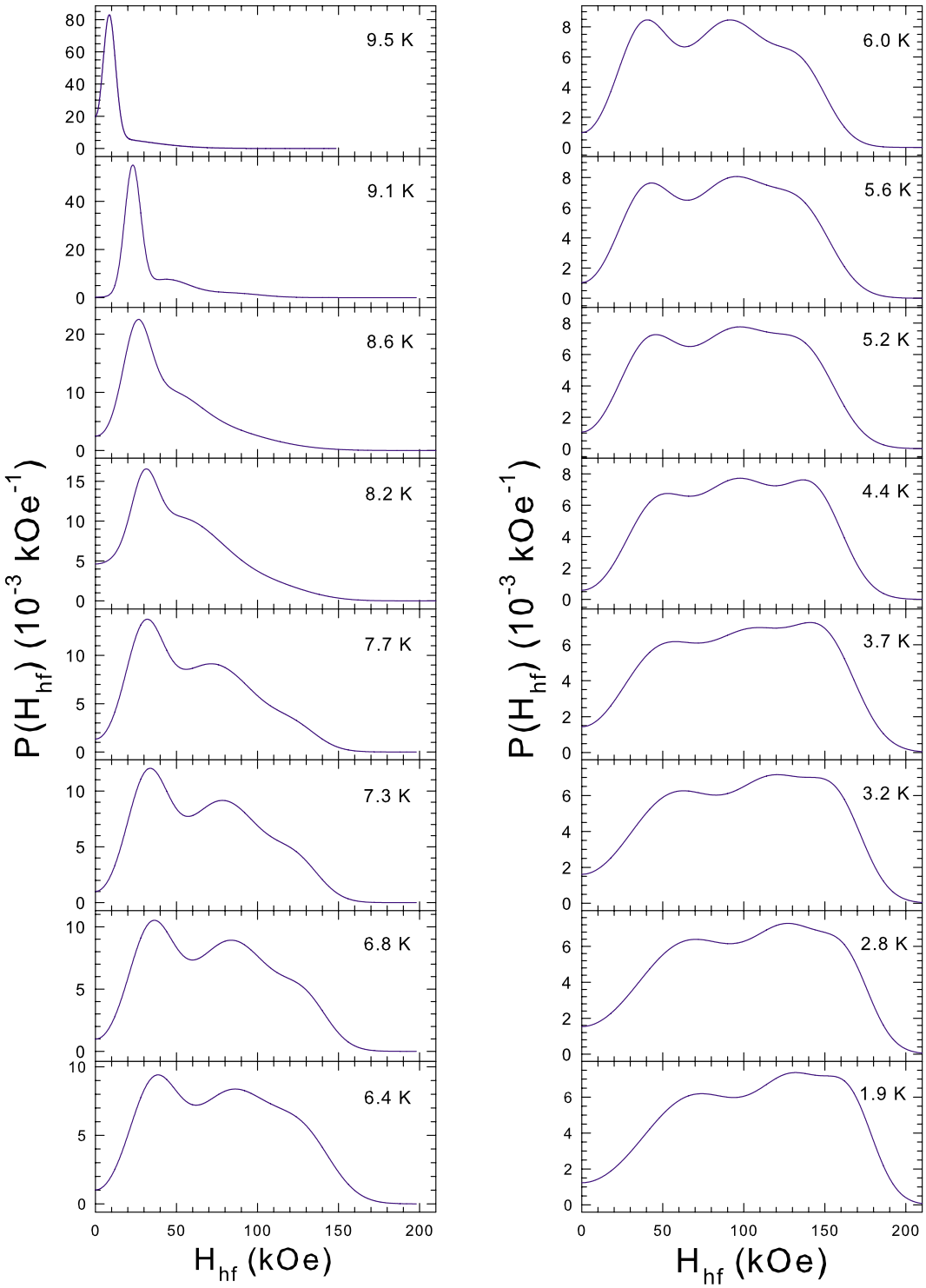

FIG. 16. (Color online) The hyperfine magnetic field distributions $P(H_{hf})$ which fit best the ^{57}Fe Mössbauer spectra in Fig. 15.

Δ for the elementary Lorentzian doublets was assumed.[52,53] The best fits of the Mössbauer spectra in Fig. 12 could be obtained with the probability quadrupole splitting probability distribution functions $P(\Delta)$ shown in Fig. 13.

The determined distributions $P(\Delta)$ (Fig. 13) clearly have a bimodal character. This is in contrast to the unimodal distribution $P(\Delta)$ observed for the thermodynamically stable i-$Al_{62.5}Cu_{24.5}Fe_{13}$ QC.[54] The bimodal character of $P(\Delta)$ may be indicative of the presence of two classes of Fe sites in the structure of the i-$Zn_{77}Fe_7Sc_{16}$ QC. The lack of *ab initio* calculations of the distribution of the EFG in the i-$Zn_{77}Fe_7Sc_{16}$ QC inhibits a comparison of the experimentally determined $P(\Delta)$ with theory. Such calculations are very desirable because the experimentally determined shape of $P(\Delta)$ could be directly used to determine which of the possible structural models of the i-$Zn_{77}Fe_7Sc_{16}$ QC is the most appropriate.

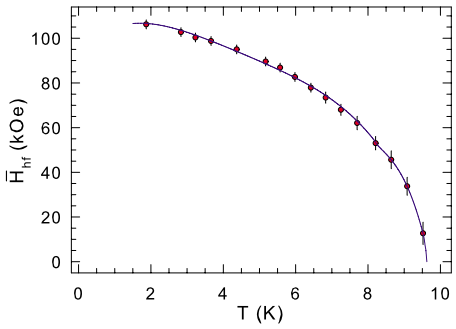

FIG. 17. (Color online) The temperature dependence of the average hyperfine magnetic field of the i-$Zn_{77}Fe_7Sc_{16}$ quasicrystal. The solid line is a guide for the eyes.

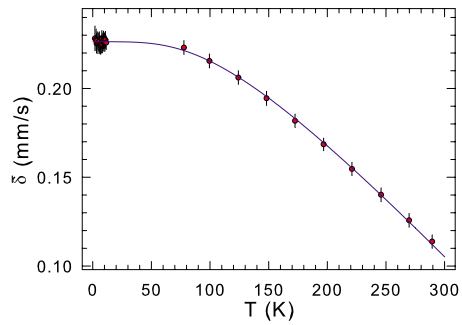

FIG. 18. (Color online) The temperature dependence of the average center shift of the i-$Zn_{77}Fe_7Sc_{16}$ quasicrystal. The solid line is the fit to Eq. (8), as explained in the text.

The average value of the quadrupole splitting, $\bar{\Delta}$, at a given temperature was calculated from the $P(\Delta)$ distribution at that temperature (Fig. 13). One can note a small increase in $\bar{\Delta}$ with decreasing temperature (Fig. 14). The temperature dependence of $\bar{\Delta}$ could be fitted well (Fig. 14) to the empirical equation

$$\bar{\Delta}(T) = \bar{\Delta}(0)(1 - BT^{3/2}), \tag{7}$$

where $\bar{\Delta}(0)$ is the value of $\bar{\Delta}$ at 0 K and B is a constant. Such a $T^{3/2}$ temperature dependence has been observed in many metallic noncubic crystalline alloys,[55] in some metallic amorphous alloys,[56,57] and recently in QCs[54,57,58] over temperature ranges from a few K to the melting point. This seemingly universal $T^{3/2}$ dependence is not well understood. Its origin seems to be associated with a strong temperature dependence of mean-square lattice displacements and, to a lesser extent, with the temperature dependence of the lattice parameters.[59] The values of $\bar{\Delta}(0)$ and B determined from the fit for the i-$Zn_{77}Fe_7Sc_{16}$ QC are, respectively, 0.527(1) mm/s and $8.87(44)\times 10^{-6}$ $K^{-3/2}$. The value of B is similar to that found for other metallic amorphous alloys and QCs.[56,58]

The Mössbauer spectra of the i-$Zn_{77}Fe_7Sc_{16}$ QC measured at temperatures at which the magnetic dipole hyperfine interaction[50] is present are shown in Fig. 15. They were fitted with the Voigt-based hyperfine magnetic field, H_{hf}, distribution method of Rancourt and Ping.[52] A linear coupling between δ and H_{hf}, and the quadrupole shift,[50] ϵ, and H_{hf}, for the elementary sextets was assumed.[52,53] The area ratio for elementary sextets, which was obtained from the fit of the 1.9 K Mössbauer spectrum, was fixed to 3:1.7:1:1:1.7:3. The best fits of the Mössbauer spectra in Fig. 15 were obtained with the hyperfine magnetic field probability distribution functions $P(H_{hf})$ shown in Fig. 16.

Similar to the case of the $P(\Delta)$ distributions, the $P(H_{hf})$ distributions are also bimodal (Fig. 16). This is suggestive of two classes of Fe sites in the structure of the i-$Zn_{77}Fe_7Sc_{16}$ QC. The structure of the 1/1 approximant Zn_6Sc can be described as a bcc array of interpenetrating triacontahedra clusters.[13] There are seven Zn sites in the Zn_6Sc structure.[13] The cluster consists of the innermost disordered tetrahedron of Zn7, a dodecahedral shell of Zn5 and Zn6, an icosahedron of Sc, and a isosidodecahedral shell of Zn3 and Zn4; Zn1 and Zn2 are located between the clusters and serve as "glue" atoms. The nearest atomic environment around the glue atoms and the Zn7 site are similar. Also the nearest atomic environments around the Zn atoms in the dodecahedral and isosidodecahedral shells are expected to be alike. There are thus two types of local atomic environments around Zn atoms. Due to similarity between the atomic radii of Fe and Zn, it is reasonable to expect that Fe atoms will occupy Zn sites in the Zn_6Sc structure. Assuming that the atomic structure of the i-$Zn_{77}Fe_7Sc_{16}$ QC consists of the same cluster building blocks as those in Zn_6Sc, one would expect the presence of two classes of Fe sites.

The average value of the hyperfine magnetic field, $\bar{H}_{hf}$, at a given temperature was calculated from the $P(H_{hf})$ distribution at that temperature (Fig. 16). The temperature dependence of $\bar{H}_{hf}$ is presented in Fig. 17. The temperature at which $\bar{H}_{hf}$ vanishes, which was estimated from the spline extrapolation of the $\bar{H}_{hf}(T)$ data in Fig. 17, is 9.60(5) K. If one defines the freezing temperature of a spin glass determined from MS, T_f^M, as the temperature at which the magnetic dipole hyperfine interaction disappears, then $T_f^M = 9.60(5)$ K. Clearly, T_f^M is significantly larger than the freezing temperature $T_f = 7.75(2)$ K determined from the dc magnetic susceptibility data. The systematically higher values of T_f^M than T_f have been observed for many other spin-glass systems.[31,60] The inequality $T_f^M > T_f$ results from a time window τ_{exp} of an experimental technique used to determine

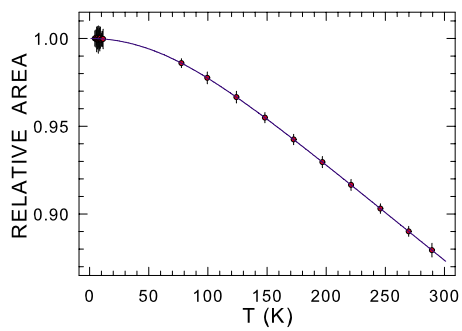

FIG. 19. (Color online) The temperature dependence of the normalized absorption area of the Mössbauer spectra of the i-$Zn_{77}Fe_7Sc_{16}$ quasicrystal. The solid line is the fit to Eq. (10), as explained in the text.

the freezing temperature. For MS, $\tau_{\rm exp}$ is given by the Larmor precession time τ_L ($\tau_L \equiv \omega_L^{-1} = \frac{\hbar I_{\rm ex}}{H_{\rm hf}\mu_{\rm ex}}$, where ω_L is the angular Larmor frequency and $I_{\rm ex}$ and $\mu_{\rm ex}$ are the spin and the magnetic moment of the excited nuclear state, respectively[61]) of the nuclear magnetic moment in the hyperfine magnetic field. In the case studied here, $\tau_L = 1.9 \times 10^{-8}$ s ($f_L = 8.4$ MHz) for $\bar{H}_{\rm hf} = 106.2$ kOe at 1.9 K. With a wide distribution of the relaxation times τ of fluctuating spin clusters in a spin glass,[31,60,62] those clusters fluctuating with τ larger than $\tau_{\rm exp}$ of a given experimental technique will appear frozen and will be discerned at a higher temperature than by the experimental technique characterized by a smaller $\tau_{\rm exp}$. Thus, one expects to observe an increase in T_f with decreasing $\tau_{\rm exp}$, which is indeed universally observed in spin glasses.[31,60]

The average center shift at temperature T, $\bar{\delta}(T)$, determined from the fits of the spectra in Figs. 12 and 15 is given by

$$\bar{\delta}(T) = \delta_0 + \delta_{\rm SOD}(T), \tag{8}$$

where δ_0 is the intrinsic isomer shift and $\delta_{\rm SOD}(T)$ is the second-order Doppler (SOD) shift which depends on lattice vibrations of the Fe atoms.[50] In terms of the Debye approximation of the lattice vibrations, $\delta_{\rm SOD}(T)$ is expressed[50] by the Debye temperature, Θ_D, as

$$\delta_{\rm SOD}(T) = -\frac{9}{2}\frac{k_B T}{Mc}\left(\frac{T}{\Theta_D}\right)^3 \int_0^{\Theta_D/T} \frac{x^3 dx}{e^x - 1}, \tag{9}$$

where M is the mass of the Mössbauer nucleus and c is the speed of light. By fitting the experimental data (Fig. 18) to Eq. (9), the quantities δ_0 and Θ_D were found to be, respectively, 0.226(1) mm/s and 443(8) K.

The absorption area $A(T)$ of a Mössbauer spectrum is proportional to the absorber Debye-Waller factor f_a given[50] by

$$f_a(T) = \exp\left\{-\frac{3}{4}\frac{E_\gamma^2}{Mc^2 k_B \Theta_D}\left[1 + \left(\frac{T}{\Theta_D}\right)^2 \int_0^{\Theta_D/T} \frac{x dx}{e^x - 1}\right]\right\}, \tag{10}$$

where E_γ is the energy of the Mössbauer transition. Figure 19 shows the temperature dependence of the relative area $A(T)/A(T_0)$ ($T_0 = 4.4$ K) derived from the fits of the Mössbauer spectra in Figs. 12 and 15. The fit of the relative area (Fig. 19) to Eq. (10) gives $\Theta_D = 455(4)$ K. This value of Θ_D is close to the value of 443(8) K derived from the $\delta_{\rm SOD}(T)$ dependence.

The Θ_D derived from the $\delta_{\rm SOD}(T)$ dependence is expected to be larger than that derived from the $f_a(T)$ dependence. This is because, in the expressions for $\delta_{\rm SOD}$ and f_a, the phonon angular frequency (ω) distribution is weighted by, respectively, ω and ω^{-1}.[63] Thus the high-ω phonons contribute more to $\delta_{\rm SOD}$ than to f_a. The similar values of Θ_D derived from the $\delta_{\rm SOD}(T)$ and $f_a(T)$ dependences may be interpreted as an indication that the phonon spectrum in the studied QC is relatively narrow. The value of Θ_D found here is comparable to the values of Θ_D found for other *i* QCs containing TM elements.[54,57,58]

IV. SUMMARY

A new thermodynamically stable *i* QC $Zn_{77}Fe_7Sc_{16}$ has been studied with x-ray diffraction, dc and ac magnetic susceptibility, and ^{57}Fe Mössbauer spectroscopy. It has a primitive six-dimensional Bravais lattice at room temperature with the six-dimensional hypercubic lattice constant of 7.087(1) Å. Based on dc magnetization measurements, it is shown that the *i* QC $Zn_{77}Fe_7Sc_{16}$ develops no long-range magnetic order in the temperature range between 2 and 300 K. The temperature dependence of the dc magnetic susceptibility follows the modified Curie-Weiss law with the paramagnetic Curie temperature at 10.6(2) K and an effective magnetic moment of 3.55(1) μ_B per Fe atom. The dc zero-field-cooled and field-cooled susceptibility data indicate that the studied QC is a spin glass with the freezing temperature $T_f = 7.75(2)$ K. This spin-glass state of the *i* QC $Zn_{77}Fe_7Sc_{16}$ is further confirmed by observing aging effects through the dc zero-field-cooled magnetization and the thermoremanent magnetization time decays and by the analysis of the frequency dependence of T_f using the Vogel-Fulcher law and the dynamic scaling behavior near T_f. However, the observed increase in the thermoremanent magnetization with the magnetic field in the low-field regime is shown to be incompatible with a highly degenerate, ultrametrically organized free-energy landscape of a canonical spin glass. The nature of the spin-glass state of the *i* QC $Zn_{77}Fe_7Sc_{16}$ is thus fundamentally different from that of a canonical spin glass. The bimodal distribution of the electric quadrupole splitting and of the hyperfine magnetic field derived from Mössbauer spectra indicates the existence of two classes of Fe sites. The decrease in the average quadrupole splitting with temperature is well described by a power-law $T^{3/2}$ relation. The hyperfine magnetic field sets in at a temperature of 9.87(5) K, which is significantly higher than T_f. The lattice vibrations of the Fe atoms are well described by a Debye model, with the Debye temperature at 453(4) K.

ACKNOWLEDGMENTS

This work was supported by the Natural Sciences and Engineering Research Council of Canada. Support from the Polish Ministry of Science and Higher Education and the Structural Funds of the European Commission (Project No. SPO WKP 1.4.3) is gratefully acknowledged.

*stadnik@uottawa.ca

[1] D. Shechtman, I. Blech, D. Gratias, and J. W. Cahn, Phys. Rev. Lett. **53**, 1951 (1984).

[2] *Physical Properties of Quasicrystals*, edited by Z. M. Stadnik (Springer-Verlag, Berlin, 1999); *Quasicrystals, an Introduction to Structure, Physical Properties, and Applications*, edited by J.-B. Suck, M. Schreiber, and P. Häussler (Springer-Verlag, Berlin, 2002).

[3] R. Lifshitz, in *Proceedings of the 5th International Conference on Quasicrystals*, edited by C. Janot and E. Mosseri (World Scientific, Singapore, 1995), p. 43; R. Lifshitz, Phys. Rev. Lett. **80**, 2717 (1998); Mater. Sci. Eng., A **294-296**, 508 (2000); R. Lifshitz and S. Even-Dar Mandel, Acta Crystallogr., Sect. A: Found. Crystallogr. **A60**, 167 (2004); S. Even-Dar Mandel and R. Lifshitz, *ibid.* **A60**, 179 (2004).

[4] C. Godrèche, J. M. Luck, and H. Orland, J. Stat. Phys. **45**, 777 (1986); S. M. Bhattacharjee, J.-S. Ho, and J. A. Y. Johnson, J. Phys. A **20**, 4439 (1987); Y. Okabe and K. Niizeki, J. Phys. Soc. Jpn. **57**, 16 (1988); M. Duneau, F. Dunlop, A. Jagannathan, and C. Oguey, Mod. Phys. Lett. B **5**, 1895 (1991); S. Matsuo, T. Ishimasa, and H. Nakano, Mater. Sci. Eng., A **294-296**, 633 (2000); J. Magn. Magn. Mater. **246**, 223 (2002); S. Matsuo, H. Nakano, S. Motomura, and T. Ishimasa, J. Phys. Soc. Jpn. **74**, 1036 (2005); S. Matsuo, S. Motomura, and T. Ishimasa, Philos. Mag. **87**, 51 (2007).

[5] D. Ledue, J. Teillet, J. Carnet, and J. Dujardin, J. Non-Cryst. Solids **153-154**, 403 (1993); R. W. Reid, K. Bose, and B. Mitrović, J. Phys.: Condens. Matter **10**, 2303 (1998); J. Hermisson, J. Phys. A **33**, 57 (2000).

[6] S. Wessel, A. Jagannathan, and S. Haas, Phys. Rev. Lett. **90**, 177205 (2003); E. Y. Vedmedenko, H. P. Oepen, and J. Kirschner, *ibid.* **90**, 137203 (2003); A. Jagannathan, *ibid.* **92**, 047202 (2004); E. Y. Vedmedenko, U. Grimm, and R. Wiesendanger, *ibid.* **93**, 076407 (2004); E. Y. Vedmedenko, Ferroelectrics **305**, 129 (2004); S. Wessel and I. Milat, Phys. Rev. B **71**, 104427 (2005); A. Jagannathan, *ibid.* **71**, 115101 (2005); E. Y. Vedmedenko, U. Grimm, and R. Wiesendanger, Philos. Mag. **86**, 733 (2006); A. Jagannathan, A. Szallas, S. Wessel, and M. Duneau, Phys. Rev. B **75**, 212407 (2007); A. Szallas and A. Jagannathan, *ibid.* **77**, 104427 (2008).

[7] A. Jagannathan and H. J. Schulz, Phys. Rev. B **55**, 8045 (1997); K. Hida, Phys. Rev. Lett. **86**, 1331 (2001).

[8] Z. M. Stadnik, G. Stroink, H. Ma, and G. Williams, Phys. Rev. B **39**, 9797 (1989); K. Fukamichi, in *Physical Properties of Quasicrystals*, edited by Z. M. Stadnik (Springer-Verlag, Berlin, 1999), p. 295; Z. M. Stadnik, Acta Phys. Pol. A **114**, 1475 (2008).

[9] B. Charrier, B. Ouladdiaf, and D. Schmitt, Phys. Rev. Lett. **78**, 4637 (1997).

[10] T. J. Sato, H. Takakura, A. P. Tsai, and K. Shibata, Phys. Rev. Lett. **81**, 2364 (1998); D. R. Noakes, G. M. Kalvius, R. Wäppling, C. E. Stronach, M. F. White, Jr., H. Saito, and K. Fukamichi, Phys. Lett. A **238**, 197 (1998); Z. Islam, I. R. Fisher, J. Zarestky, P. C. Canfield, C. Stassis, and A. I. Goldman, Phys. Rev. B **57**, R11047 (1998).

[11] T. J. Sato, H. Takakura, A. P. Tsai, K. Shibata, K. Ohoyama, and K. H. Andersen, Phys. Rev. B **61**, 476 (2000); T. J. Sato, H. Takakura, A. P. Tsai, K. Ohoyama, K. Shibata, and K. H. Andersen, Mater. Sci. Eng., A **294-296**, 481 (2000); T. J. Sato, H. Takakura, J. Guo, A. P. Tsai, and K. Ohoyama, J. Alloys Compd. **342**, 365 (2002); T. J. Sato, Acta Crystallogr., Sect. A: Found. Crystallogr. **A61**, 39 (2005); T. J. Sato, H. Takakura, A. P. Tsai, and K. Shibata, Phys. Rev. B **73**, 054417 (2006).

[12] Q. Lin and J. D. Corbett, Philos. Mag. Lett. **83**, 755 (2003); R. Maezawa, S. Kashimoto, and T. Ishimasa, *ibid.* **84**, 215 (2004).

[13] Q. Lin and J. D. Corbett, Inorg. Chem. **43**, 1912 (2004).

[14] H. Takakura, C. P. Gómez, A. Yamamoto, M. de Boissieu, and A. P. Tsai, Nature Mater. **6**, 58 (2007).

[15] S. Kashimoto, S. Motomura, R. Maezawa, S. Matsuo, and T. Ishimasa, Jpn. J. Appl. Phys., Part 2 **43**, L526 (2004); S. Kashimoto, S. Motomura, S. Francoual, S. Matsuo, and T. Ishimasa, Philos. Mag. **86**, 725 (2006).

[16] D. L. Bish and S. J. Chipera, Powder Diffr. **4**, 137 (1989).

[17] W. Wong-Ng and C. R. Hubbard, Powder Diffr. **2**, 242 (1987).

[18] S. W. Freiman and N. M. Trahey, *Standard Reference Material 640c, Silicon Powder Line Position and Line Shape Standard for X-ray Diffraction* (National Institute of Standards and Technology, Gaithersburg, 2000).

[19] L. H. Lewis and K. M. Bussmann, Rev. Sci. Instrum. **67**, 3537 (1996).

[20] *Certificate of Calibration, Iron Foil Mössbauer Standard*, Natl. Bur. Stand. (U.S.) Circ. No. 1541, edited by J. P. Cali (U.S. GPO, Washington, D.C., 1971).

[21] R. Jenkins and W. N. Schreiner, Powder Diffr. **4**, 74 (1989).

[22] W. N. Schreiner and R. Jenkins, Adv. X-Ray Anal. **26**, 141 (1983).

[23] J. W. Cahn, D. Shechtman, and D. Gratias, J. Mater. Res. **1**, 13 (1986).

[24] V. Elser, Acta Crystallogr., Sect. A: Found. Crystallogr. **A42**, 36 (1986).

[25] P. A. Bancel, P. A. Heiney, P. W. Stephens, A. I. Goldman, and P. M. Horn, Phys. Rev. Lett. **54**, 2422 (1985).

[26] J. Banhart, H. Ebert, J. Voitländer, and H. Winter, J. Magn. Magn. Mater. **61**, 221 (1986).

[27] D. Mandrus, J. L. Sarrao, A. Migliori, J. D. Thompson, and Z. Fisk, Phys. Rev. B **51**, 4763 (1995).

[28] Ž. Bihar, A. Bilušić, J. Lukatela, A. Smontara, P. Jeglič, P. J. McGuiness, J. Dolinšek, Z. Jagličić, J. Janovec, V. Demange, and J. M. Dubois, J. Alloys Compd. **407**, 65 (2006).

[29] M. B. Maple, E. D. Bauer, V. S. Zapf, and J. Wosnitza, in *Superconductivity, Conventional and Unconventional Superconductors*, edited by K. H. Bennemann and J. B. Ketterson (Springer, Berlin, 2008), Vol. 1, p. 639.

[30] Y. Ishii, K. Nozawa, and T. Fujiwara, Philos. Mag. **86**, 693 (2006).

[31] J. A. Mydosh, *Spin Glasses: An Experimental Introduction* (Taylor & Francis, London, 1993).

[32] L. Lundgren, P. Svedlindh, P. Nordblad, and O. Beckman, Phys. Rev. Lett. **51**, 911 (1983).

[33] R. V. Chamberlin, G. Mozurkewich, and R. Orbach, Phys. Rev. Lett. **52**, 867 (1984); R. Hoogerbeets, W.-L. Luo, and R. Orbach, *ibid.* **55**, 111 (1985); M. A. Continentino and A. P. Malozemoff, Phys. Rev. B **33**, 3591 (1986).

[34] R. V. Chamberlin, Phys. Rev. B **30**, 5393 (1984).

[35] M. Lederman, R. Orbach, J. M. Hammann, M. Ocio, and E. Vincent, Phys. Rev. B **44**, 7403 (1991).

[36] D. Chu, G. G. Kenning, and R. Orbach, Philos. Mag. B **71**, 479 (1995).

[37] G. Parisi, Phys. Rev. Lett. **50**, 1946 (1983).

[38] M. Mézard, G. Parisi, N. Sourlas, G. Toulouse, and M. Virasoro,

J. Phys. (Paris) **45**, 843 (1984).
[39] S. Kirkpatrick and D. Sherrington, Phys. Rev. B **17**, 4384 (1978).
[40] S. F. Edwards and P. W. Anderson, J. Phys. F: Met. Phys. **5**, 965 (1975).
[41] D. J. Thouless, P. W. Anderson, and R. G. Palmer, Philos. Mag. **35**, 593 (1977).
[42] A. J. Bray and M. A. Moore, J. Phys. C **13**, L469 (1980).
[43] M. Mézard and M. A. Virasoro, J. Phys. (Paris) **46**, 1293 (1985).
[44] V. S. Dotsenko, J. Phys. C **18**, 6023 (1985).
[45] I. R. Fisher, K. O. Cheon, A. F. Panchula, P. C. Canfield, M. Chernikov, H. R. Ott, and K. Dennis, Phys. Rev. B **59**, 308 (1999).
[46] J. L. Tholence, Solid State Commun. **35**, 113 (1980).
[47] S. Shtrikman and E. P. Wohlfarth, Phys. Lett. **85A**, 467 (1981).
[48] P. C. Hohenberg and B. I. Halperin, Rev. Mod. Phys. **49**, 435 (1977).
[49] J. Souletie and J. L. Tholence, Phys. Rev. B **32**, 516 (1985).
[50] N. N. Greenwood and T. C. Gibb, *Mössbauer Spectroscopy* (Chapman and Hall, London, 1971); P. Gütlich, R. Link, and A. Trautwein, *Mössbauer Spectroscopy and Transition Metal Chemistry* (Springer, Berlin, 1978).
[51] Z. M. Stadnik, in *Mössbauer Spectroscopy Applied to Magnetism and Materials Science*, edited by G. J. Long and F. Grandjean (Plenum, New York, 1996), Vol. 2, p. 125.
[52] D. G. Rancourt and J. Y. Ping, Nucl. Instrum. Methods Phys. Res. B **58**, 85 (1991).
[53] S. J. Campbell and F. Aubertin, in *Mössbauer Spectroscopy Applied to Inorganic Chemistry*, edited by G. J. Long and F. Grandjean (Plenum, New York, 1989), Vol. 3, p. 183.
[54] Z. M. Stadnik, T. Takeuchi, N. Tanaka, and U. Mizutani, J. Phys.: Condens. Matter **15**, 6365 (2003).
[55] E. N. Kaufmann and R. H. Vianden, Rev. Mod. Phys. **51**, 161 (1979), and references therein.
[56] P. Deppe and M. Rosenberg, Hyperfine Interact. **15-16**, 735 (1983); M. Kopcewicz, B. Kopcewicz, and U. Gonser, J. Magn. Magn. Mater. **66**, 79 (1987); M. Mao, D. H. Ryan, and Z. Altounian, Hyperfine Interact. **94**, 2163 (1994).
[57] Z. M. Stadnik, J. Saida, and A. Inoue, Ferroelectrics **250**, 297 (2001); Z. M. Stadnik, Ö. Rapp, V. Srinivas, J. Saida, and A. Inoue, J. Phys.: Condens. Matter **14**, 6883 (2002).
[58] R. A. Brand, J. Voss, and Y. Calvayrac, Mater. Sci. Eng., A **294-296**, 666 (2000); Z. M. Stadnik and G. Zhang, J. Phys.: Condens. Matter **17**, 6599 (2005); R. A. Brand, F. Hippert, and B. Frick, *ibid.* **21**, 045405 (2009).
[59] K. Nishiyama, F. Dimmling, Th. Kornrumph, and D. Riegel, Phys. Rev. Lett. **37**, 357 (1976); J. Christiansen, P. Heubes, R. Keitel, W. Klinger, W. Loeffler, W. Sandner, and W. Witthuhn, Z. Phys. B **24**, 177 (1976); P. Jena, Phys. Rev. Lett. **36**, 418 (1976).
[60] A. P. Murani, J. Magn. Magn. Mater. **5**, 95 (1977); **22**, 271 (1981); H. G. Wagner and U. Gonser, *ibid.* **31-34**, 1343 (1983); C. Meyer, F. Hartmann-Boutron, Y. Gros, and I. A. Campbell, *ibid.* **46**, 254 (1985); H. Aruga, T. Tokoro, and A. Ito, J. Phys. Soc. Jpn. **57**, 261 (1988); J. Bogner, M. Reissner, W. Steiner, and S. M. Dubiel, J. Phys.: Condens. Matter **10**, 9849 (1998).
[61] J. G. Stevens, in *CRC Handbook of Spectroscopy*, edited by J. W. Robinson (CRC Press, Boca Raton, 1981), Vol. III, p. 403.
[62] L. Lundgren, P. Svedlindh, and O. Beckman, J. Phys. F: Met Phys. **12**, 2663 (1982).
[63] R. M. Housley and F. Hess, Phys. Rev. **164**, 340 (1967).